Dependence of NO rotational photoionization propensity rules on electron kinetic energy

Xinbei Song, Ellen Sekreta, and James P. Reilly
Department of Chemistry, Indiana University, Bloomington, Indiana 47405

H. Rudolph and V. McKoy
Arthur Amos Noyes Laboratory of Chemical Physics[a] *California Institute of Technology, Pasadena, California 91125*

(Received 1 May 1989; accepted 7 August 1989)

In order to study the effect of photoelectron kinetic energy on rotational photoionization propensity rules, rotationally resolved laser photoelectron spectra were measured for excitation of specific rovibronic levels in the $D\,^2\Sigma^+$ $(3p\sigma)$ Rydberg state of NO and their subsequent ionization by radiation at several wavelengths. The measured and calculated ion rotational branching ratios both show a significant dependence on photoelectron energy. Comparison between experimental data and theoretical calculations suggests that a strong $\Delta N = 0$ peak in the spectra is caused by an interaction between particular vibronic levels of the $A\,^2\Sigma^+$ $(v = 4)$ and $D\,^2\Sigma^+$ $(v = 0)$ Rydberg states.

INTRODUCTION

In recent years, the technique of resonant enhanced multiphoton ionization (REMPI) combined with high resolution photoelectron spectroscopy (PES) has proven useful in elucidating both the characteristics of intermediate electronic states and the dynamics of excited-state photoionization.[1-19] While considerable interest has been focused on the vibrational state distribution of the ions formed, and how that relates to differences between excited state and ion potential energy surfaces, a few recent experiments have achieved rotational resolution in the photoelectron spectra and provided valuable insight into the propensity rules for these processes.[4,6,10,12] These experiments are possible because specific single rovibrational levels of a certain electronic state can be excited with a pulse of narrowband laser radiation, the excited molecule ionized with the same light pulse, and the kinetic energies of the ejected electrons measured with a resolution sufficient to resolve the different rotational states of the ions. This approach to extracting rotational photoionization propensity rules has several advantages over photoionization of ground state molecules. First, ionization takes place from a single rotational state rather than from a thermal distribution of rotational levels, so the resulting spectra are simpler to interpret. Second, different types of electronic states can be excited and their varying characteristics probed. Third, by using different colors of light for the excitation and ionization steps, it is possible to study the effect of ionizing wavelength, and thus electron kinetic energy, on the rotational propensity rules.

Selection rules governing the changes in rotational angular momentum, ΔN, of a diatomic molecule upon ionization can be obtained via angular momentum and parity considerations.[6,20,21] Although such selection rules provide no information about the relative intensities of the peaks predicted to appear in a particular spectrum, they have been useful in interpreting our earlier experimental results on NO.[10,12] In particular, they correctly predict the observed $\Delta N = 0, \pm 2$ propensity when ionizing from the $A\,^2\Sigma^+$ $(3s\sigma)$ state, and the $\Delta N = 0, \pm 2$ and $\Delta N = 0, \pm 3$ propensities observed when ionizing from different spin components of the $C\,^2\Pi(3p\pi)$ state. However, when ionizing from the $D\,^2\Sigma^+$ $(3p\sigma)$ state of NO, in addition to the anticipated $\Delta N = \pm 1, \pm 3$ peaks, we observed a very intense and unexpected $\Delta N = 0$ peak.[12] Although the simplest explanation for such a peak in the photoelectron spectrum is that the $D\,^2\Sigma^+$ $(3p\sigma)$ Rydberg state might have a non-negligible amount of s character, SCF calculations conclusively demonstrated that this was not the case.[12,21,22] We then suggested, and through calculations later verified, that l mixing in the continuum can lead to a detectable $\Delta N = 0$ peak.[12,23,24] The fact that the $\Delta N = 0$ peak completely vanished when the photoelectron spectrum was recorded with light polarized perpendicular to the electron flight direction[12] is consistent with this hypothesis. Calculations further suggested that the relative magnitudes of all of the observed peaks, including the $\Delta N = 0$ feature, must depend on the kinetic energy of the ejected electron, and that this effect is much more pronounced in ionization of the $D\,^2\Sigma^+$ $(3p\sigma)$ state of NO than the $A\,^2\Sigma^+$ $(3s\sigma)$ state.[23,24] In the present work, a particular rotational level of the $D\,^2\Sigma^+$ $(3p\sigma)$ state is excited and photoelectron spectra measured with one of five different ionizing wavelengths. Calculations predicting the observed rotational state distributions are performed for precisely the photoionization wavelengths used experimentally. Although comparison of the predicted and observed spectra is encouraging, several discrepancies remain suggesting that a proper description of the $D\,^2\Sigma^+$ $(3p\sigma)$ electronic state of NO may be more complicated than had been anticipated.

EXPERIMENTAL

In our previous rotationally resolved photoelectron experiments, selected rotational levels of the $D\,^2\Sigma^+$ state of NO were reached by a two-photon process, and one addi-

[a] Contribution no. 7920.

 0021-9606/89/226062-09$02.10

tional photon was sufficiently energetic to induce ionization. The high light intensities required to two-photon excite the $D\,^2\Sigma^+$ state very efficiently ionized the excited molecules. This high photoionization efficiency becomes a problem in any two-color experiment in which the photoionization wavelength is varied; ionization of the NO by the intense light that two-photon excited it cannot be avoided. To circumvent this problem we chose in the present experiments to excite the $D\,^2\Sigma^+$ state of NO by a one-photon process using light at approximately 1871 Å. Since the lifetime of the $D\,^2\Sigma^+$ state of NO is known to be rather short (about 20 ns),[25] very little time jitter between the excitation and tunable photoionization light pulses can be tolerated. This suggests that a single pump laser should be used to generate both the excitation and ionization radiation needed in these experiments. The method employed is schematically displayed in Fig. 1. A Quanta Ray Nd:YAG laser acted as our primary light source producing 1.064 μm radiation with a repetition rate of 10 Hz. This radiation was frequency doubled in a Quanta Ray Model HG-2 harmonic generator. The resulting 532 nm light pumped a rhodamine 6G dye laser whose output was frequency doubled and mixed with the fundamental of the YAG laser in a Quanta Ray wavelength extension system (WEX). Wavelengths in the region of 2210–2230 Å were thus obtained. The output from the WEX was focused near the center of a high pressure (200 psi) hydrogen Raman shifting cell. The beams emerging from the Raman cell were collimated by a lens and dispersed by an equilateral prism. The first and second anti-Stokes lines and the first through fifth Stokes lines were all observed. The light wavelengths and pulse energies for all of these lines are listed in Table I. The second anti-Stokes line at 1871 Å was appropriate for initially exciting the $D\,^2\Sigma^+(3p\sigma)$ Rydberg state. This radiation was refracted directly into the spectrometer by a second equilateral prism. The other Stokes lines, used as ionizing radiation, were reflected by four right angle prisms and focused into the spectrometer in a counterpropagating direction. The light arrived in the photoelectron spectrometer 4 ns after the initial excitation pulse. The plane of polarization of all radiation was parallel to the electron flight direction. The reason that perpendicular polarization was not also used in the present experiment, as in the past,[12] is that the count rate in the perpendicular direction is much smaller, so these experiments take longer than the parallel polarization experiments, and it was difficult to stabilize the complicated nonlinear optical light production for such extended periods. In addition, the small signals obtained in the perpendicular direction could hardly be distinguished from the spectrometer photoemission background.

In order to know when we were exciting a particular rotational level of the $D\,^2\Sigma^+$ excited electronic state, it was necessary to record and assign a wavelength scan of an entire vibrational band. The $D\,^2\Sigma^+ \leftarrow X\,^2\Pi$ 0–0 band was recorded using a $1+1'$ REMPI process with the second anti-Stokes and the second Stokes radiation produced as described above. During the wavelength scan, acceleration grids were used to collect a substantial fraction of the electrons generated.

Nitric oxide gas (Matheson Grade CP) was purified by several freeze–thaw cycles to remove residual air and other oxides of nitrogen. An effusive beam of NO was streamed through a 30 μm nozzle into the ionization chamber of the photoelectron spectrometer which was maintained at a pressure of 5.0×10^{-5} Torr by a CTI model CRYO-TORR 8 high vacuum pump. The spectrometer, which operates on the time of flight principle, has been previously described.[26] The second anti-Stokes radiation was tuned to a particular $D\,^2\Sigma^+ \leftarrow X\,^2\Pi$ rovibrational line to excite molecules that were then ionized with one of the eight available UV and visible colors. Electrons were detected with two Varian-8900 microchannel plates in tandem. The resulting signals were amplified and digitized with a Biomation 6500 waveform recorder and LeCroy 2228A and 4208 time to digital converters (TDCs) with time resolution of 250 ps per channel and 1 ns per channel, respectively. The data were stored in a PCs Limited AT-compatible computer. Spectra were subsequently converted from linear in time to linear in kinetic energy and then transferred to a plotter.

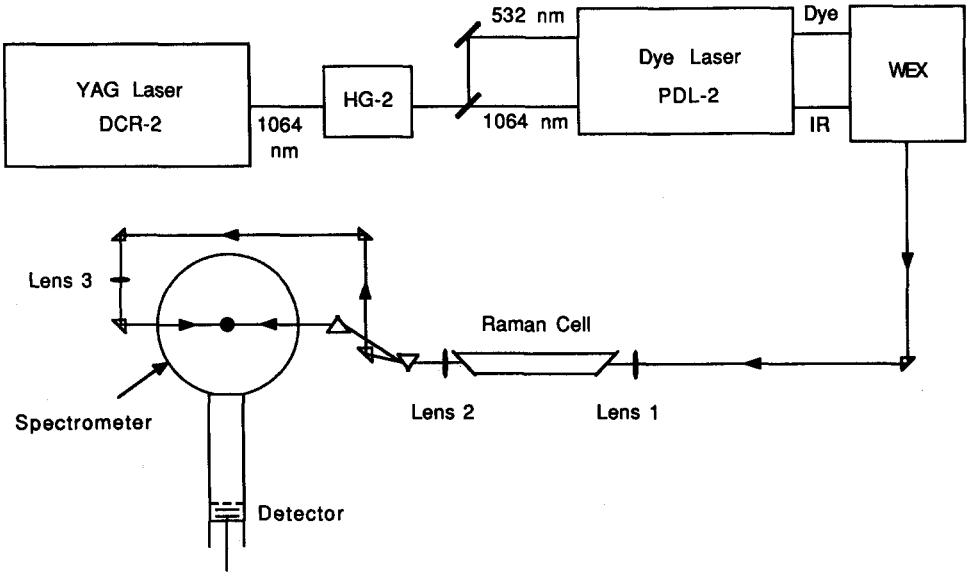

FIG. 1. Apparatus employed to generate UV laser radiation and to record time of flight laser photoelectron spectra. WEX is a Quanta Ray wavelength extension system. MCP is the microchannel plate detector.

TABLE I. Photon and electron energetics.

Raman line	Ionizing λ (Å)	Pulse energy (μJ)	Photon E (eV)	Electron K.E.[a] (eV)
2nd anti-Stokes	1871	2.4	6.626	3.940
1st anti-Stokes	2029	···	6.111	3.425
Main beam	2216	320	5.596	2.910
1st Stokes	2440	240	5.081	2.395
2nd Stokes	2716	160	4.565	1.879
3rd Stokes	3061	60	4.050	1.364
4th Stokes	3507	12	3.535	0.849
5th Stokes	4106	0.8	3.020	0.334

[a] Electron kinetic energy was calculated for $\Delta N = 0$ peak of each photoelectron spectrum.

THEORETICAL

The $(1+1')$ REMPI via the $D\,^2\Sigma^+$ state of NO,

$$\mathrm{NO}[X\,^2\Pi(v''=0,J'')] \xrightarrow{h\nu} \mathrm{NO}^*[D\,^2\Sigma^+(v'=0,J'N')]$$

$$\xrightarrow{h\nu'} \mathrm{NO}^+[X\,^1\Sigma^+(v_+=0,J_+N_+)] + e^-(\mathbf{k}) \qquad (1)$$

can be viewed as a two-step process: a one-photon excitation from an initially unaligned $X\,^2\Pi$ ground state (all M_J levels equally populated) to the aligned $D\,^2\Sigma^+$ intermediate state, followed by subsequent one-photon ionization out of this aligned state. Details of the theory of molecular REMPI processes used in these studies have been described in Ref. 27, while the general aspects of REMPI of NO have been discussed in Refs. 20 and 21.

Under the collision-free conditions of the current experiments alignment of the resonant state is preserved and each (allowed) M_J channel can be treated as an independent ionization channel. The total probability $P(\theta,\phi)$ for photoelectron ejection in the direction (θ,ϕ) with respect to the polarization vector $(\boldsymbol{\varepsilon})$ of the laser light is given by

$$P(\theta,\phi) = \sum_{J'} \sum_{M_{J'}} \Gamma_{M_{J'}M_{J'}}\, \rho_{M_{J'}M_{J'}}\,, \qquad (2)$$

where the incoherent sum over allowed J' levels accounts for the mixed rotational branches via the $D\,^2\Sigma^+$ state $(J' = N' \pm 1/2)$ [e.g., $Q_{21} + R_{11}(J')$], $\Gamma_{M_{J'}M_{J'}}$, is the ionization probability out of the $M_{J'}$ level, and $\rho_{M_{J'}M_{J'}}$ its population. For the low intensity experiments of interest here, $\rho_{M_{J'}M_{J'}}$ is adequately described by a product of 3-j coefficients and the line strength $A(J'', N'', J', N')$[28]

$$\rho_{M_{J'}M_{J'}} \propto \begin{pmatrix} J'' & 1 & J' \\ M_{J'} & 0 & M_{J'} \end{pmatrix}^2 A(J'',N'',J',N'). \qquad (3)$$

The photoionization probability $P(\theta)$ can be expanded in Legendre polynomials $P_L[\cos(\theta)]$ as

$$P(\theta) = \sum_{L=0}^{L_{\max}/2} \beta_{2L} P_{2L}[\cos(\theta)]. \qquad (4)$$

For the present two-photon $(1+1')$ REMPI study, with relatively high values of J' and low laser intensity, $L_{\max}$ is 4. The photoelectron signal detected along the direction of polarization of the laser is therefore $P(\theta = 0°) = \beta_0 + \beta_2 + \beta_4$, and the perpendicular signal is $P(\theta = 90°) = \beta_0 - \frac{1}{2}\beta_2 + \frac{3}{8}\beta_4$.

The electronic wave function for the intermediate $D\,^2\Sigma^+$ state is obtained via diagonalization of the static-exchange potential associated with the $X\,^1\Sigma^+$ ground state of NO^+.[12,22,24,29] We used the same Gaussian basis as in Ref. 24, except that the functions at the center of mass (CM) were taken from Ref. 22 (s, p, and d functions with exponents larger than 0.0008). This basis gives a calculated total energy of $-129.035\,87$ a.u. for the $D\,^2\Sigma^+(3p\sigma)$ state at $R = 2.0069$ a.u. A partial wave decomposition of the resulting $3p\sigma$ orbital about the CM gives 0.6% s, 98.8% p, 0.4% d, and 0.1% f character, respectively, in agreement with previous calculations.[12,20,24] This same basis set gives a total energy of $-129.073\,63$ a.u. for the $A\,^2\Sigma^+(3s\sigma)$ state at $R = 2.0069$ a.u., and a single-center expansion of the $3s\sigma$ orbital around the CM of 94.0% s, 0.2% p, 5.5% d, and 0.1% f character, respectively.

Determination of the M_J resolved photoionization probability $\Gamma_{M_{J'}M_{J'}}$ involves sums of the square of the bound–free matrix elements $r_{fi}^{l\lambda\mu}$,

$$r_{fi}^{l\lambda\mu} = \sum_{l',l_0} \langle \Psi_{kll'}(r)\, Y_{l'\lambda}(\hat{r}') | r Y_{l\mu}(\hat{r}') | \Phi_{il_0}(r)\, Y_{l_0 0}(\hat{r}') \rangle \qquad (5)$$

between the resonant Rydberg and photoelectron orbitals. The photoelectron continuum functions are calculated using the iterative Schwinger variational method.[30,31] These photoelectron orbitals are obtained as solutions of a one-electron Schrödinger equation containing the nonspherical, nonlocal potential of the molecular ion. The partial wave coupling in these molecular photoelectron orbitals is important for the description of the nonatomic nature of molecular photoionization. All matrix elements are evaluated for a fixed internuclear distance of $R = 2.0069$ a.u. corresponding to the equilibrium distance of the $^2\Sigma^+$ Rydberg states.[32]

RESULTS AND DISCUSSION

The wavelength dependence of the NO^+ ion yield is displayed in Fig. 2(a). The simulation of this band, obtained using spectroscopic constants of NO that are known in both the ground and excited vibronic states,[32] is shown in Fig. 2(b). This simulation assumes that the $D\,^2\Sigma^+$ state is described by Hund's case (b) and that the $X\,^2\Pi$ state is inter-

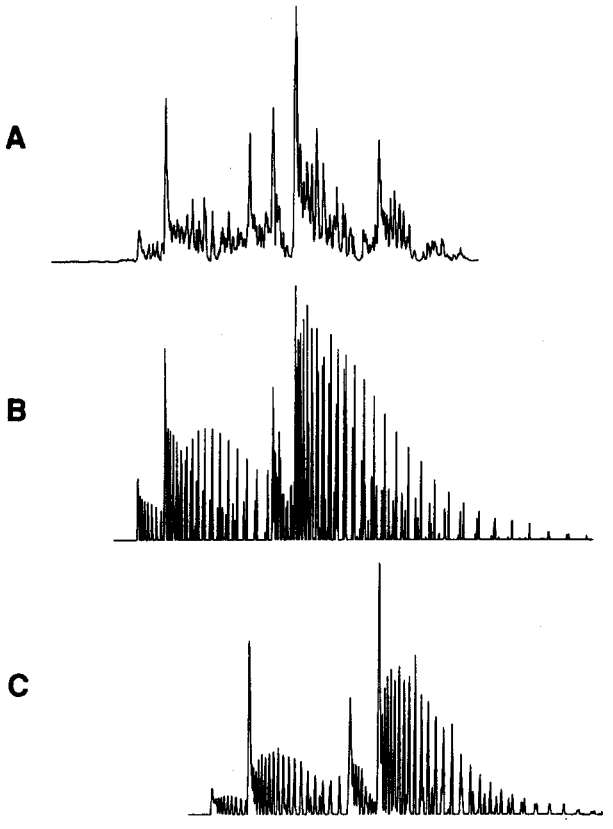

FIG. 2. (A) Wavelength dependence of NO ionization yield obtained under effusive beam conditions using the second anti-Stokes line to excite and the second Stokes to ionize. (B) The calculated simulation of the rotational structure of the $D\,^2\Sigma^+ \leftarrow X\,^2\Pi$ 0–0 band. (C) The calculated simulation of the rotational structure of the $A\,^2\Sigma^+ \leftarrow X\,^2\Pi$ 4–0 band.

mediate between Hund's cases (a) and (b).[33] There is a 119.7 cm^{-1} separation between the $X\,^2\Pi_{1/2}$ and $X\,^2\Pi_{3/2}$ levels of the NO ground state, leading to $D\,^2\Sigma^+ \leftarrow X\,^2\Pi_{1/2}$ and $D\,^2\Sigma^+ \leftarrow X\,^2\Pi_{3/2}$ subbands. In addition, the interaction between rotation of the nuclei and electronic orbital angular momentum (Λ doubling) splits each rotational level of the Π state into two components. Because of the large energy-level separation in the NO ground state, the selection rule $\Delta N = 0, \pm 1$ does not apply and all transitions consistent with the selection rule $\Delta J = 0, \pm 1$ and $+ \leftrightarrow -$ are possible. Therefore, $R_1, Q_1, P_1, {}^SR_{21}, {}^RQ_{21}$, and ${}^QP_{21}$ branches are formed from $X\,^2\Pi_{1/2}$ levels, and $R_2, Q_2, P_2, {}^QR_{12}, {}^PQ_{12}$, and ${}^OP_{12}$ branches from the $X\,^2\Pi_{3/2}$ level. The intensities of the rotational lines were calculated using Earls' equation.[28] As can be seen from a comparison of Figs. 2(a) and 2(b), it is quite evident that an additional transition must be occurring in this wavelength region. This transition can be assigned as the $A\,^2\Sigma^+ \leftarrow X\,^2\Pi$ 4–0 band whose absolute position and rotational structure were calculated from other known spectroscopic constants. A simulation of the $A\,^2\Sigma^+ \leftarrow X\,^2\Pi$ 4–0 band is separately displayed in Fig. 2(c). In the absorption spectrum of nitric oxide between 1700 and 2300 Å, the $D\,^2\Sigma^+ \leftarrow X\,^2\Pi$ 0–0 band, the $A\,^2\Sigma^+ \leftarrow X\,^2\Pi$ 4–0 band and the $B\,^2\Pi \leftarrow X\,^2\Pi$ 8–0 band have been found to be overlapped.[34] The former two bands are more intense than the third. The presence of this overlapping absorption introduced considerable congestion into the spectrum and severely limits the number of nonoverlapping rotational transitions that can be cleanly excited. Nevertheless, towards the short wavelength end of the spectrum it was possible to assign a rather weak, relatively resolvable feature. An expanded view of this area of the spectrum is displayed in Fig. 3. Based on the slit function used in our spectral simulation, it is possible to estimate that the linewidth of our tunable VUV radiation was about 1.2 cm^{-1}.

The particular spectral line that we chose to focus on (labeled "II" in Fig. 3) actually involves two overlapping transitions: R_1 (17.5) and ${}^RQ_{21}$ (17.5). This line was selected because of its relatively small overlap with lines in the $A\,^2\Sigma^+ \leftarrow X\,^2\Pi$ (4,0) band referred to previously. Although the two overlapping transitions involve different J levels in the $D\,^2\Sigma^+$ state, the rotational quantum number N in both of these upper levels is 18. Therefore, this mixed line can be used to study rotational photoionization propensities.

With approximately 2.4 μJ of the second antistokes radiation alone we recorded the photoelectron spectrum displayed in Fig. 4. As can be seen from Table I, with such a short ionizing wavelength the kinetic energies of the ejected electrons are near 4 eV, and our TOF electron spectrometer's resolution is insufficient to distinguish ions generated in different rotational states. Nevertheless, it is quite apparent that ions are being produced in more than one vibrational state. The separation between the two principal features displayed in Fig. 4 is approximately 1.15 eV, which corresponds to the separation between the $v = 0$ and $v = 4$ ion vibrational states. Since the Franck-Condon factor connecting the $v = 4$ level of an ion with the $v = 0$ level of an excited Rydberg state is extremely small, the most likely explanation for their appearance is that there is sufficient overlap between the $D\,^2\Sigma^+ \leftarrow X\,^2\Pi$ (0,0) and $A\,^2\Sigma^+ \leftarrow X\,^2\Pi$ (4,0) bands so that a substantial fraction of the initially excited molecules are in the A state. This could be due to over-

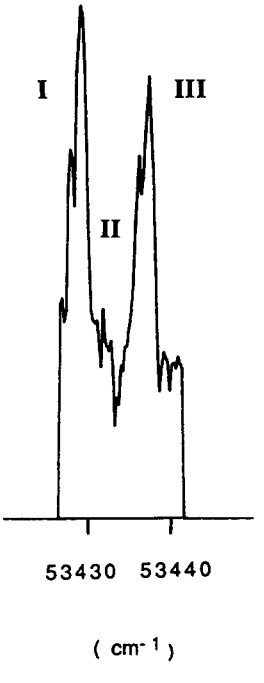

FIG. 3. Wavelength scan near the region of the R_1 (17.5) + ${}^RQ_{21}$ (17.5) mixed line of the 0–0 band of the $D\,^2\Sigma^+ \leftarrow X\,^2\Pi$ transition. Peak I involves the R_1 (12.5), ${}^RQ_{21}$ (12.5) and ${}^SR_{21}$ (7.5) lines of the $A\,^2\Sigma^+ \leftarrow X\,^2\Pi$ 4–0 band. Peak II is the R_1 (17.5) + ${}^RQ_{21}$ (17.5) mixed line of the $D\,^2\Sigma^+ \leftarrow X\,^2\Pi$ 0–0 band. Peak III is the result of overlapping R_1(13.5), ${}^RQ_{21}$(13.5), and ${}^SR_{21}$(8.5) lines of the $A\,^2\Sigma^+ \leftarrow X\,^2\Pi$ 4–0 band.

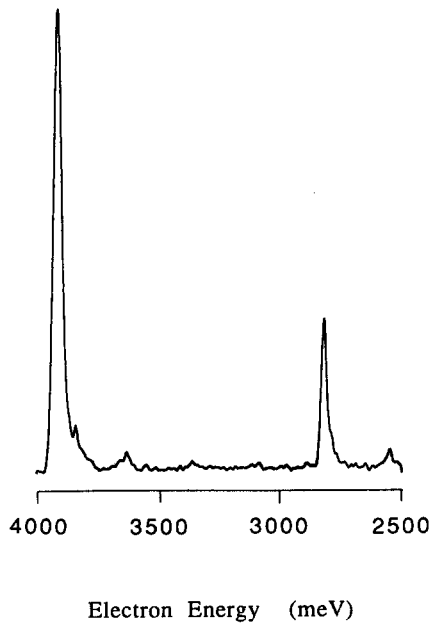

FIG. 4. Photoelectron spectrum recorded with laser tuned to peak II of Fig. 3.

lapping spectral transitions or simply because the $v = 0$ level of the $D\,^2\Sigma^+$ state vibronically mixes with the nearby $v = 4$ level of the $A\,^2\Sigma^+$ state. The latter hypothesis will be further considered below.

The limited electron energy resolution attainable when electrons are ejected with rather substantial kinetic energies is not the only problem associated with using short wavelength radiation. A second one is that the light induces a substantial photoemission that appears as a background over a wide range of electron energies. Because of these two problems we did not record two-color laser photoelectron spectra with either the fundamental or the first anti-Stokes line. Instead, we concentrated on photoionizing with the first, second, third, fourth, and fifth Stokes lines whose wavelengths and photon energies are listed in Table I. In order to record these two-color photoelectron spectra, it was important to strictly limit the fluence of second anti-Stokes radiation with a small aperture, while using substantially higher intensity Stokes radiation pulses. In this way, most of the $D\,^2\Sigma^+$ state NO molecules were ionized with Stokes light.

Photoelectron spectra obtained by exciting with the second anti-Stokes line and ionizing with the fifth, fourth, third, second, and first Stokes lines are displayed in Figs. 5(A)–5(E). Only that part of each spectrum corresponding to ions produced in their ground vibrational state is displayed. Although in a few cases the peaks corresponding to $v = 4$ ions were rotationally resolved, the resulting rotational state distributions were not so simple as those associated with $v = 0$ ions since no effort was made to excite a single level characterized by just one N quantum number.

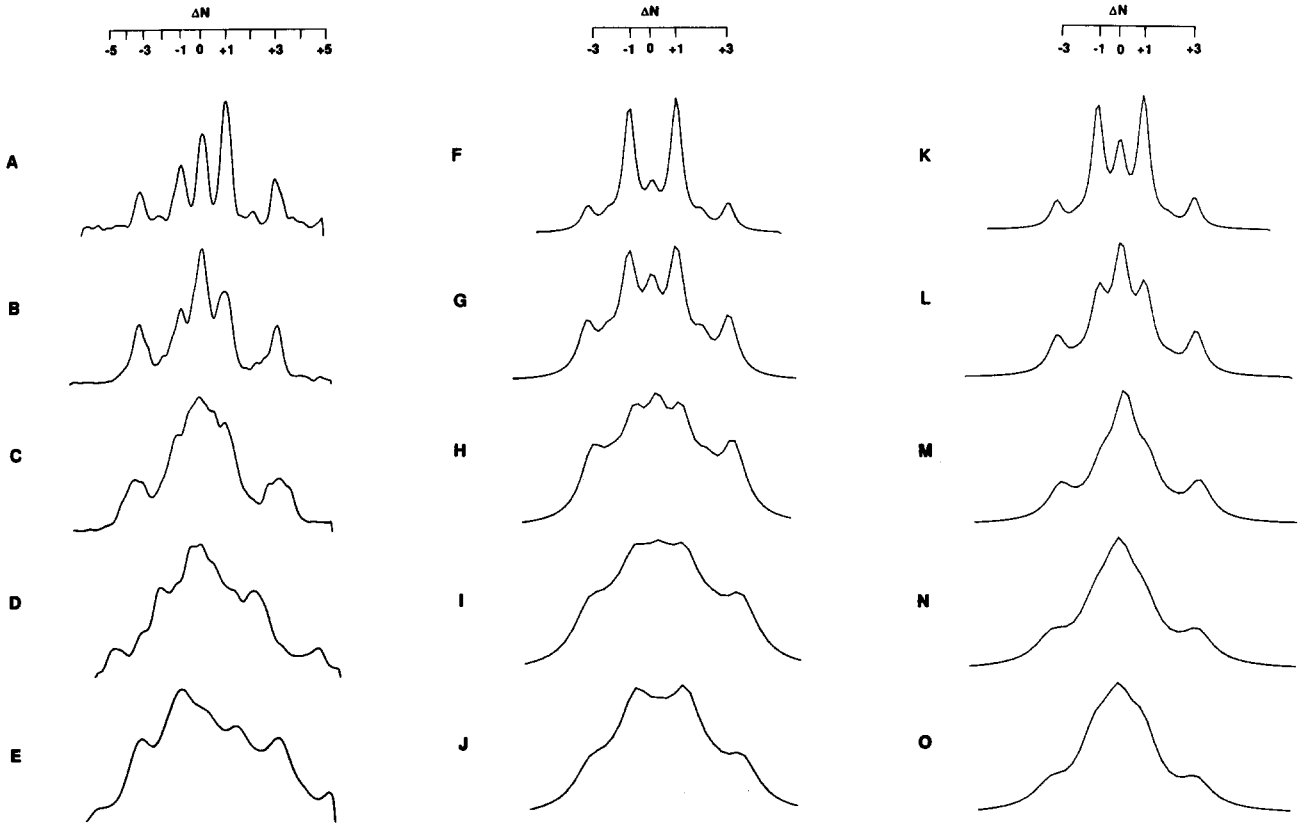

FIG. 5. Comparison of experimentally observed and theoretically predicted photoelectron spectra obtained by exciting the $R_1(17.5) + {}^RQ_{21}(17.5)$ mixed line of the $D\,^2\Sigma^+ \leftarrow X\,^2\Pi$ transition. (A)–(E) Experimental data obtained by exciting with the second anti-Stokes line and ionizing with the fifth, fourth, third, second and first Stokes lines respectively. (F)–(J) Spectra calculated by assuming the same photoelectron kinetic energies as in Fig. 5 (A)–(E). (K)–(O) Spectra calculated by assuming mixing between $A\,^2\Sigma^+$ and $D\,^2\Sigma^+$ Rydberg states.

We have previously studied branching ratios for $(2+1)$ REMPI via the $D\,^2\Sigma^+$ state.[12,24] The agreement between the calculated and measured branching ratios was quite good except for an anomalously strong $\Delta N=0$ signal seen experimentally for parallel ($\theta=0$) photoelectron detection, indicating, by virtue of the selection rule $\Delta N+l=$ odd, the presence of a strong p wave in the continuum.[21] Our calculated rotational branching ratios and total cross sections for $(2+1')$ REMPI of NO via the $D\,^2\Sigma^+$ state were also highly dependent on the photoelectron kinetic energy. The branching ratios of the present $(1+1')$ REMPI experiments can also be expected to display a similar dependence on photoelectron energy. Figure 5 shows the experimental (A)–(E) and calculated (F)–(J) branching ratios for parallel detection in $(1+1')$ REMPI via the mixed $Q_{21}+R_{11}(17.5)$ branch of the $D\,^2\Sigma^+$ state. These calculated branching ratios have been convoluted with a Lorentzian detector function with a FWHM determined from the experimental resolution (5.5–14 meV). The measured and calculated branching ratios are strongly dependent on the photoelectron kinetic energy. The $\Delta N=0$ signal is significant at all photoelectron energies and most dominant at $\sim$0.85eV. The high ΔN peaks (±4, ±5), experimentally observed at higher kinetic energies, are not seen in the calculated spectra. In the calculated branching ratios the $\Delta N=0$ signal is significant throughout the whole energy range but not as dominant as seen experimentally. The presence of the $\Delta N=0$ signal in the calculated branching ratios probes the $l=1$ character of the photoelectron orbital. To illustrate this, we give the partial wave decomposition of the bound-free matrix elements, proportional to $|r_{fi}^{l\lambda\mu}|^2$, as a function of l and energy in Table II. The $k\pi$ channel is dominant at lower energies. Further, as expected from an atomic-like photoionization picture ($l=l_0\pm1$), the d wave ($l=2$) is substantial throughout. The $p\sigma$ wave ($l=1$, $m_l=0$) is, however, far from negligible and is primarily responsible for the $\Delta N=0$ signal.

At these low energies the $\Delta N=0$ signal is a measure of the contribution of the $l=1$ wave of the photoelectron orbital to the transition moment. Comparison of the predicted and measured $\Delta N=0$ signals indicates that this component of the photoelectron matrix element is being underestimated in the calculations. Our experience in studies of REMPI of other $^2\Sigma^+$ states of NO suggests that this behavior is not due to inaccuracies in the photoelectron orbitals.[12,22,24,35] The vibronic spectrum of the D state shows some differences from that of the other Rydberg states which suggest a possible explanation for these discrepancies. As a Rydberg state the D state is expected to have vibrational constants similar to those of the $NO^+\ X\,^1\Sigma^+$ ground state, despite the slight antibonding character of the 7σ orbital, i.e. $\omega_e\cong2376\ cm^{-1}$ and $\omega_e x_e\cong16\ cm^{-1}$.[32] The D state's vibrational constants are, however, $\omega_e\cong2324\ cm^{-1}$ and $\omega_e x_e\cong23\ cm^{-1}$.[32] The $v_D=0$ level is almost degenerate with the $v_A=4$ level of the $A\,^2\Sigma^+$ state suggesting possible perturbations between these $v_D=0$ and $v_A=4$ levels. Several perturbations have been identified among the Rydberg states of NO,[36–41] but, to our knowledge, perturbations between the $v_D=0$ and $v_A=4$ levels have not been addressed. The D state is known to be perturbed in different parts of the vibronic manifold, e.g., the complicated indirect hetereogeneous perturbation between the $B\,^2\Pi\sim C\,^2\Pi\sim L\,^2\Pi\sim D\,^2\Sigma^+$ states[40–42] and the possible perturbation by the dissociative $A'\,^2\Sigma^+$ $(2p''\sigma_u'')$ state.[37,43] Neither of these perturbations can give rise to the almost pure s character ($l_0=0$) in the resonant electronic state necessary to explain the anomalously large $\Delta N=0$ signal arising from $l=1$ character of the photoelectron wave function since the $^2\Pi$ states and the $A'\,^2\Sigma^+$ state have essentially no s character.

This apparently direct homogeneous Rydberg–Rydberg perturbation between the A and D states is unusual, since they have different "atomic symmetries" (l_0), $3s\sigma$ and $3p\sigma$, and it does not obey the vibrational propensity rule for Rydberg–Rydberg interactions: $\Delta v=\pm1$.[42] But similar interactions have been found in the PO molecule (valence-shell-isoelectronic with NO) by Ngo *et al.*[44] for the corresponding states $A\,^2\Sigma^+(4s\sigma,v=12)$ and $H\,^2\Sigma^+$ $(4p\sigma,v=0)$. This perturbation arises via second-order van Vleck corrections with a leading term from interactions with the $F\,^2\Sigma^+$ valence state.[42] It is possible that similar interactions are present in the NO molecule. However, there is insufficient spectroscopic data to sustain this theory.

A determination of the interaction of the $v_A=4$ and $v_D=0$ levels would require a careful deperturbation study, as described by Lefebvre–Brion,[42] or a knowledge of highly accurate potential curves so far only obtainable for H_2.[45] Assuming the two Rydberg states interact, the only good quan-

TABLE II. Value of $|r_{fi}^{l\lambda\mu}|^2$ as a function of l, normalized to the dominant wave for each energy.

		E(eV) Photoelectron energy				
	l	0.33	0.85	1.36	1.88	2.35
	0	0.0880	0.1544	0.3864	0.3340	0.3278
	1	0.1472	0.2647	0.4914	0.2886	0.1984
$k\sigma$	2	0.0146	0.2113	0.9785	≡1.00	≡1.00
	3	0.0129	0.0247	0.0457	0.0260	0.0174
	4	0.0003	0.0005	0.0009	0.0005	0.0003
	1	0.0053	0.0090	0.0167	0.0098	0.0066
$k\pi$	2	≡1.00	≡1.00	≡1.00	0.2807	0.0747
	3	0.0192	0.0396	0.0765	0.0448	0.0301
	4	0.0001	0.0001	0.0002	...	...

tum numbers would be parity, energy, and the rotational quantum number J. A crude model for the effect of the perturbation is to allow the two adiabatic electronic wave functions $\Psi_A^{\text{ad.}}$ and $\Psi_D^{\text{ad.}}$ to mix, forming an "effective" diabatic wave function for the D state,

$$\Psi_D = c_1\Psi_D^{\text{ad.}} + c_2\Psi_A^{\text{ad.}}, \tag{6}$$

where $c_2 = (1 - c_1^2)^{1/2}$. In the present frozen-core approximation this amounts to a mixing of the 6σ and 7σ orbitals. Assuming the two sublevels, $N' \pm 1/2$, in the D state have the same coupling, we can assess the perturbation from the strength of the observed $\Delta N = 0$ signal. We determine c_1 and c_2 by adjusting them so as to reproduce the observed branching ratio $\eta \equiv (\Delta N = 0)/(\Delta N = +1)$ of ~ 1.5 at 0.85 eV. This give values of $c_1 = 0.990$ and $c_2 = 0.142$, i.e., Ψ_D ($\nu_D = 0, J' = 17.5, 18.5$) level is $\sim 98\%$ "D state" and $\sim 2\%$ "A state." Single-center expansion of this state yields a 2.8% s, 96.7% p, and 0.3% d character.

In Fig. 5(K)–(O) we show the calculated branching ratios using this mixed state for parallel detection of $(1 + 1')$ REMPI via the mixed $Q_{21} + R_{11}(17.5)$ branch of the $D\,^2\Sigma^+$ state. The calculated branching ratios are again convoluted with a Lorentzian detector function with a FWHM determined from the experimental resolution. The agreement between the experimental and the calculated results is much better than for the unperturbed state. The calculated $\Delta N = 0$ signal now increases with increasing photoelectron energy and the intensity of the $\Delta N = \pm 3$ peaks decreases going from 0.85 to 1.36 eV photoelectron kinetic energy. This is primarily due to the insensitivity of the A state component's cross section to photoelectron energy for this perturbed state and to the strong energy dependence of the D state component. The significant increase in the $\Delta N = 0$ signal for this mixed D state, arising from the small ($\sim 2\%$) admixture of the A state, is due to the very strong $\Delta N = 0$ propensity rule of the A state, as observed experimentally in $(1 + 1)$ REMPI via the $A\,^2\Sigma^+(3s\sigma)$ state.[10,12,13]

A few experimentally observed trends are not reproduced so well in the calculated spectra. The calculated spectra do not show the same strong asymmetry at low photoelectron kinetic energy (0.33 eV) nor the high angular momentum transfer peaks ($\Delta N = \pm 4, \pm 5$) at higher energies (1.88 and 2.39 eV) seen experimentally. In Table III we show the calculated, normalized, partial wave decomposition of the bound-free matrix elements, proportional to $|r_{fi}^{l\lambda\mu}|^2$, for the $k\sigma$ and $k\pi$ channels The p wave is, as expected, more dominant for this "mixed" state, and the angular distribution for the $\Delta N = 0$ signal, dominated by this component, therefore has a large β_2 value. In Fig. 6 we show the calculated branching ratios for detection perpendicular to the polarization for the perturbed, Fig. 6 (a)–(e), and the unperturbed D state, Fig. 6 (f)–(j). The two sets of results are virtually identical, reflecting the perpendicular signals' insensitivity ($\cos^2\theta$) to the presence of the $l_0 = 0$ component in the resonant state. This is in agreement with our earlier experimental[12] and theoretical[24] results for $(2 + 1)$ REMPI via the $S_{21}(11.5)$ and $R_{21} + S_{11}(15.5)$ branches of $D\,^2\Sigma^+$ state, where agreement between the experimental and theoretical results was excellent for perpendicular detection. However, the strong $\Delta N = 0$ signal observed experimentally in parallel detection,[12] was not well-reproduced theoretically.[24]

Other mechanisms for the presence of the strong $\Delta N = 0$ signal include correlation effects in the intermediate state that may introduce s-character into the $D\,^2\Sigma^+$ state. Bergeman and Zare[39] have measured the effective dipole moment of the $A\,^2\Sigma^+$ ($\nu_A = 3$) state to be $|\mu^{\text{exp}}| = 1.10 \pm 0.03$ D, which differs significantly from the SCF value, $\mu^{\text{SCF}} = 0.66$ D ($N^{\delta+}O^{\delta-}$), and that of earlier configuration interaction (CI) calculations,[46] $\mu \cong 0.40$ D. Bergeman and Zare attribute this disagreement to possible perturbations between the $A\,^2\Sigma$ and the $D\,^2\Sigma^+$ states, either by "dipole borrowing" or nonadiabatic couplings possibly via the repulsive $A'\,^2\Sigma^+$ state[43] consistent with the assumptions we have made here. More extensive CI calculations have since determined the dipole moment of the $A\,^2\Sigma^+$ state to be ~ 1.4 D,[47,48] a value much closer to the experimental value. The transition moments between the Rydberg states are known, however, to be quite insensitive to inclusion of correlation effects,[12,49] and the CI calculated dipole moment for the $D\,^2\Sigma^+$ state $\mu^{\text{CI}} = -2.2$ D ($N^{\delta} - O^{\delta+}$)[47] agrees well with the value obtained from the present IVO calculations $\mu^{\text{IVO}} = -2.0$ D. Furthermore if this were purely an adiabatic electronic effect, and therefore independent of J' and N', the mixed D state obtained above should then be suitable for describing branching ratios for other rotational branches of the D state. A calculation of the branching ratios via the

TABLE III. Value of $|r_{fi}^{l\lambda\mu}|^2$ as a function of l, for ionization via mixed D state, normalized to the dominant wave for each energy.

		E(eV) (Photoelectron energy)				
	l	0.33	0.85	1.36	1.88	2.39
	0	0.0791	0.1539	0.3632	0.3275	0.3311
	1	0.1930	0.3767	0.6556	0.4151	0.3088
$k\sigma$	2	0.0203	0.2634	≡1.00	≡1.00	≡1.00
	3	0.0010	0.0008	0.0010	0.0033	0.0059
	4	0.0002	0.0005	⋯	0.0006	0.0005
	1	0.0475	0.1111	0.2256	0.1622	0.1330
$k\pi$	2	≡1.00	≡1.00	0.8639	0.2394	0.0620
	3	0.0034	0.0047	0.0041	0.0009	0.0004
	4	0.0001	0.0002	0.0002	⋯	⋯

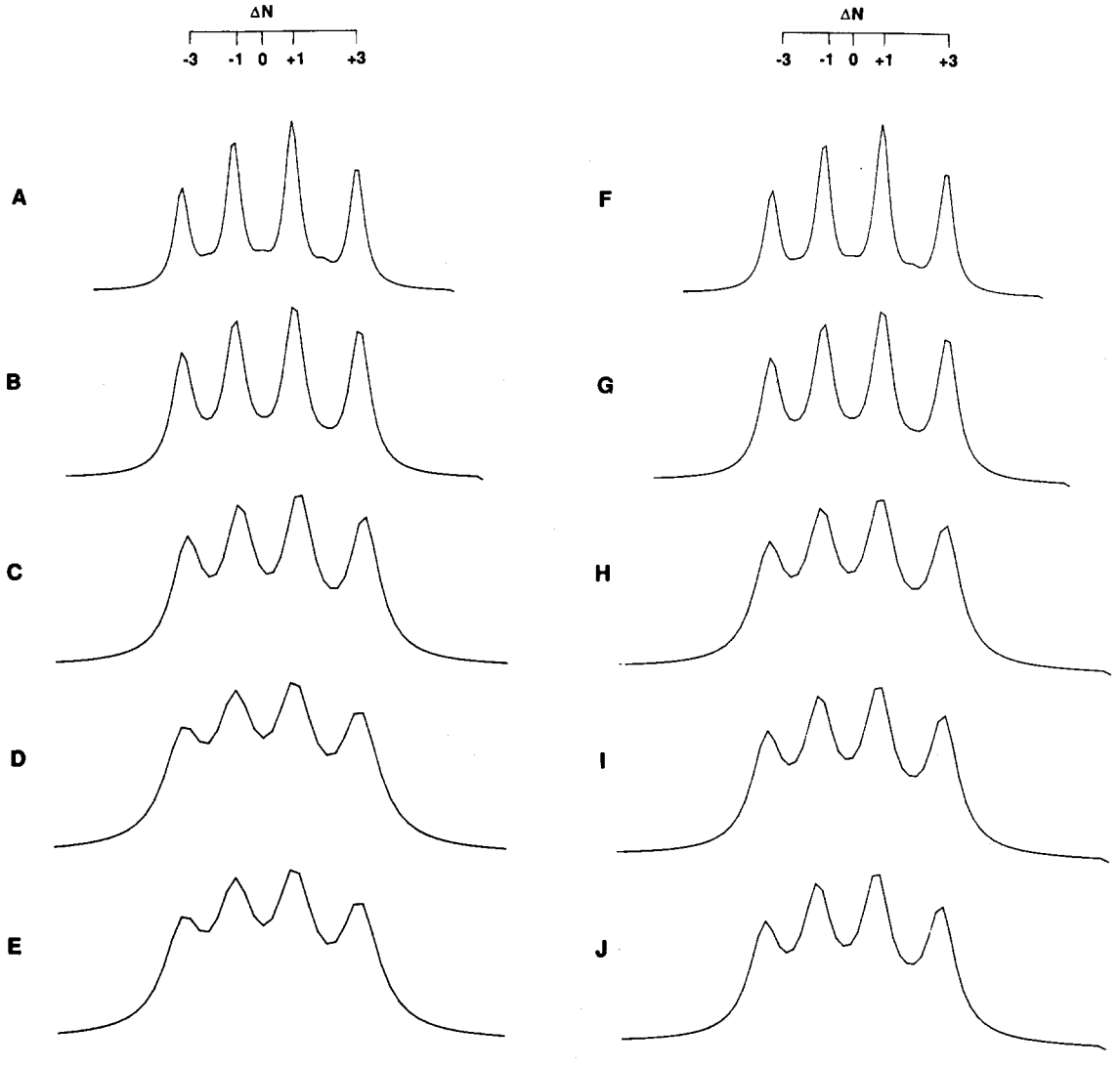

FIG. 6. Calculated branching ratios for (1 + 1′) REMPI via the $R_1(17.5) = {}^RQ_{21}(17.5)$ branch of the $D\,^2\Sigma^+$ state of NO, assuming the same photoelectron kinetic energies as in Fig. 5 (a)–(e). Detection perpendicular to the polarization of the light ($\theta = 90°$). (a)–(e) Calculated assuming no mixing between the $A\,^2\Sigma^+$ and $D\,^2\Sigma^+$ states. (f)–(j) Calculated assuming the existence of mixing between $A\,^2\Sigma^+$ and $D\,^2\Sigma^+$ states, see text for details.

previously studied $S_{21}(11.5)$ and $R_{21} + S_{11}(17.5)$ branches[12] with this perturbed D state leads however to a poorer agreement with the experimental results. Finally, it could be due to final state effects such as autoionization, predissociation, etc. However, the agreement between theory and experiment over an energy range of ~2 eV, using the perturbed intermediate state does not support this possibility. We therefore believe the "dynamic" coupling between the A and D state is a likely cause of the large $\Delta N = 0$ signal observed here.

The obvious asymmetry that is displayed in the experimental spectrum of Fig. 5(A) but is missing from its theoretical counterparts [Figs. 5(F) and 5(K)] is highly reproducible and perhaps noteworthy. There are a few reasons why it is not likely to be due to variations in the electron spectrometer transmission. First, our spectrometer's transmission tends to cut off between 50 and 100 meV, depending on its condition, which is well below the lowest energy peak (~300 meV) in Fig. 5(A). Second, the asymmetry in the middle of the spectrum involving the $\Delta N = +1$ and -1 peaks appears to be more dramatic than at the edges where the $\Delta N = +3$ and -3 peaks are involved. Third, the $\Delta N = -1$ peak, which appears to be smaller than the $\Delta N = +1$ peak, actually occurs at higher electron energy than the latter and thus is less likely to be discriminated against. Finally, the asymmetry is also present to a small degree in Fig. 5(B) and to a considerable degree in Figs. 9(a) and 10(a) of Ref. 13. The combination of these facts suggests that the observed asymmetry is a real effect and not an experimental artifact.

ACKNOWLEDGMENTS

The research at Indiana University was supported by the National Science Foundation under Grant No. CHE-8800991. The research at the California Institute of Technology was supported by the National Science Foundation under Grant No. CHE-8521391, by AFOSR under Grant No. 87-0039, and by the Office of Health and Environmental Research of DOE (DE-FGO3-87ER60513). The authors

also acknowledge use of the resources of the San Diego SuperComputer Center which is supported by the National Science Foundation. H.R. and V.M. would like to thank Dr. H. Lefebvre-Brion and Dr. R. Cave for helpful discussions. H.R. gratefully acknowledges the support of the Danish Natural Science Research Council and a NATO Science Fellowship.

[1]J. T. Meek, S. R. Long, and J. P. Reilly, J. Phys. **86**, 2809 (1982).
[2]S. L. Anderson, D. M. Rider, and R. N. Zare, Chem. Phys. Lett. **93**, 11 (1982).
[3]J. Kimman, P. Krust, and M. J. Van der Wiel, Chem. Phys. Lett. **88**, 576 (1982).
[4]J. E. Pollard, D. J. Trevor, J. E. Reutt, Y. T. Lee, and D. A. Shirley, J. Chem. Phys. **77**, 34 (1982).
[5]S. R. Long, J. T. Meek, and J. P. Reilly, J. Chem. Phys. **79**, 3206 (1983).
[6]S. T. Pratt, P. M. Dehmer, and J. L. Dehmer, J. Chem. Phys. **78**, 4315 (1983).
[7]P. Kruit, H. G. Muller, J. Kimman, and M. J. Van der Wiel, J. Phys. B **16**, 2359 (1983).
[8]Y. Achiba, K. Sato, K. Shobatake, and K. Kimura, J. Chem. Phys. **78**, 5474 (1983).
[9]S. L. Anderson, G. D. Kubiak, and R. N. Zare, Chem. Phys. Lett. **105**, 22 (1984).
[10]W. G. Wilson, K. S. Viswanathan, E. Sekreta, and J. P. Reilly, J. Phys. Chem. **88**, 672 (1984).
[11]J. Kimman, M. Lavollee, and M. J. Van der Wiel, Chem. Phys. **97**, 137 (1985).
[12]K. S. Viswanathan, E. Sekreta, E. R. Davidson, and J. P. Reilly, J. Chem. Phys. **90**, 5078 (1986).
[13]K. S. Viswanathan, E. Sekreta, and J. P. Reilly, J. Phys. Chem. **90**, 5658 (1986).
[14]A. Sur, C. V. Ramana, W. A. Chupka, and S. D. Colson, J. Chem. Phys. **84**, 69 (1986).
[15]T. M. Orlando, L. Li, S. L. Anderson, and M. G. White, Chem. Phys. Lett. **129**, 31 (1986).
[16]J. C. Miller and R. N. Compton, J. Chem. Phys. **84**, 675 (1986).
[17]J. Kimman, J. W. J. Verschuur, M. Lavollee, H. B. van Linden van den Heuvell, and M. J. van der Wiel, J. Phys. B **19**, 3909 (1986).
[18]P. Chen, J. B. Pallix, W. A. Chupka, and S. D. Colson, J. Chem. Phys. **86**, 516 (1987).
[19]D. T. Biernacki, E. E. Eyler, and S. D. Colson, J. Chem. Phys. **88**, 2099 (1988).
[20]S. N. Dixit, D. L. Lynch, V. McKoy, and W. M. Huo, Phys. Rev. A **32**, 1267 (1985).
[21]S. N. Dixit and V. McKoy, Chem. Phys. Lett. **128**, 49 (1986).
[22]K. Kaufmann, C. Nager, and M. Jungen, Chem. Phys. **95**, 385 (1985).
[23]H. Rudolph, S. N. Dixit, V. McKoy, and W. M. Huo, Chem. Phys. Lett. **137**, 521 (1987).
[24]H. Rudolph, S. N. Dixit, V. McKoy, and W. M. Huo, J. Chem. Phys. **88**, 637 (1988).
[25]A. B. Callear, M. J. Pilling, and I. W. M. Smith, Trans. Faraday Soc. **64**, 2296 (1968).
[26]S. R. Long, J. T. Meek, J. P. Reilly, J. Chem. Phys. **79**, 3206 (1983).
[27]S. N. Dixit and V. McKoy, J. Chem. Phys. **82**, 3546 (1985).
[28]L. T. Earls, Phys. Rev. **48**, 423 (1935).
[29]W. J. Hunt and W. A. Goddard III, Chem. Phys. Lett. **24**, 464 (1974).
[30]R. R. Lucchese, G. Raseev, and V. McKoy, Phys. Rev. A **25**, 2572 (1982).
[31]R. R. Lucchese, K. Takatsuka, and V. McKoy, Phys. Rep. **131**, 147 (1986).
[32]K. P. Huber and G. Herzberg, *Constants of Diatomic Molecules* (Van Nostrand Reinhold, New York, 1979).
[33]J. B. Halpern, H. Zacharias, and R. Wallenstein, J. Mol. Spectrosc. **79**, 1 (1980).
[34]G. W. Bethke, J. Chem. Phys. **31**, 662 (1959).
[35]H. Rudolph, S. N. Dixit, V. McKoy, and W. M. Huo, J. Chem. Phys. **88**, 1516 (1988).
[36]C. Jungen and E. Miescher, Can. J. Phys. **46**, 987 (1968).
[37]E. Miescher, Can. J. Phys. **49**, 2350 (1971).
[38]Y. Ben-Aryeh, J. Quant. Spectrosc. Radiat. Transfer. **13**, 1441 (1973).
[39]T. Bergeman and R. N. Zare, J. Chem. Phys. **61**, 4500 (1974).
[40]R. Gallusser and K. Dressler, J. Chem. Phys. **76**, 4311 (1982).
[41]J. Kimman, M. Laollêe and M. J. Van der Wiel, Chem. Phys. **97**, 137 (1985).
[42]H. Lefebvre-Brion and R. W. Field *Perturbations in the Spectra of Diatomic Molecules* (Academic, New York, 1986).
[43]F. R. Gillmore, J. Quant. Spectr. Radiat. Transfer. **5**, 369 (1965).
[44]T. A. Ngo, M. DaPaz, B. Coquart, C. Couet, Can. J. Phys. **52**, 154 (1974).
[45]K. Dressler, R. Gallusser, P. Quadrelli, and L. Wolniewicz, J. Mol. Spectrosc. **75**, 205 (1979).
[46]S. Green, Chem. Phys. Lett. **23**, 115 (1973).
[47]S. P. Walch and W. A. Goddard III, Chem. Phys. Lett. **33**, 18 (1975).
[48]S. R. Langhoff, C. W. Bauschlicher, Jr., and H. Partridge, J. Chem. Phys. **89**, 4909 (1988).
[49]R. de Vivic and S. D. Peyerimhoff, J. Chem. Phys. **89**, 3028 (1988).